UNIVERSIDADE DE SÃO PAULO

INSTITUTO DE FÍSICA
CAIXA POSTAL 20516
01498 - SÃO PAULO - SP
BRASIL

publicações

IFUSP/P-473

NEAR/FAR DECOMPOSITION OF THE PROTON-NUCLEUS AND ANTIPROTON-NUCLEUS ELASTIC SCATTERING ANGULAR DISTRIBUTIONS

by

B.V. Carlson and M.P. Isidro Filho
Divisão de Física Teórica, Instituto de Estudos Avançados, Centro Técnico Aeroespacial, 12200 São José dos Campos, SP, Brasil

and

M.S. Hussein
Instituto de Física, Universidade de São Paulo

Julho/1984

NEAR/FAR DECOMPOSITION OF THE PROTON-NUCLEUS AND ANTIPROTON-NUCLEUS ELASTIC SCATTERING ANGULAR DISTRIBUTIONS

B.V. Carlson and M.P. Isidro Filho

Divisão de Física Teórica, Instituto de Estudos Avançados, Centro Técnico Aeroespacial, 12200 São José dos Campos, SP, Brasil

and

M.S. Hussein*

Instituto de Física, Universidade de São Paulo, C.P. 20516, São Paulo, SP, Brasil

Abstract:

The elastic scattering of protons and antiprotons from nuclei at intermediate energies is discussed using the near-side/far-side decomposition of the Dirac eikonal amplitude. It is suggested that, whereas the p + A scattering system is predominantly absorptive, the $\bar{p}$ + A system exhibits strong refractive effects, leading to a far-side dominance in the angular distributions. Applications are made to several systems.

*Supported in part by the CNPq.

June/1984

In a recent paper[1] we have proposed that the anti-proton-nucleus scattering system can be successfully described by charge conjugating the Dirac equation that describes the proton-nucleus system. This charge conjugation changes the complex scalar V_s and the fourth component of the vector, V_0 potentials, usually employed to describe proton scattering from N=Z, spin saturated systems, into V_s^* and $-V_0^*$, respectively. The good agreement we obtained with the $\bar{p} + {}^{12}C$ data[2] in the beam momentum range 400-1000 $\frac{MeV}{c}$, convinced us of the adequacy of this prescription.

In this Letter, we further explore this charge conjugate duality. In particular, we look into the general structure of the elastic angular distribution for the p+A and $\bar{p}$+A systems. We do this by employing the near-side/far-side decomposition of the elastic scattering amplitude[3]. Owing to the very strong central attraction in $\bar{p}$+A, the angular distribution in the small angle region is completely dominated by the far-side piece, in great contrast to p+A system, where nuclear refractive effects are small and accordingly the near-side and far-side contributions are almost equal in magnitude giving rise to the well-known Fraunhoffer oscillations.

We start with the Dirac eikonal formulation of the proton-nucleus scattering problem as developed by Amado et al.[4]. The 2×2 matrix amplitude is then given by

$$F_p(\vec{k},\vec{k}';\epsilon) = F_{1,p}(\vec{k},\vec{k}';\epsilon) + \vec{\sigma}\cdot\hat{n}\, F_{2,p}(\vec{k},\vec{k}';\epsilon) \qquad (1)$$

where

$$F_{1,p} = -ik\int_0^\infty db\, b\, J_0(qb)\left(e^{t_c^p(b)}\cosh t_{so}^p(b) - 1\right) \quad (2)$$

$$F_{2,p} = -k\int_0^\infty db\, b\, J_1(qb)\, e^{t_c^p(b)}\sinh t_{so}^p(b) \quad (3)$$

and $\vec{\sigma}$ are the Pauli spin matrices.

In the above Equations the functions $t_c^p(b)$ and $t_{s0}^p(b)$ are given by

$$t_c^p(b) = \frac{-i}{2(\hbar c)^2 k}\int_{-\infty}^{\infty} dz'\,(N_p^2 - F_p^2 + E^2 - m^2) \quad (4)$$

$$t_{so}^p(b) = \frac{-ib}{2}\int_{-\infty}^{\infty} dz'\,\frac{1}{F_p + N_p}\,\frac{1}{r}\,\frac{d}{dr}(F_p + N_p) \quad (5)$$

$$F_p \equiv E - V_0(\vec{b}, z) \quad (6)$$

$$N_p \equiv m + V_s(\vec{b}, z) \quad (7)$$

Notice that the combination $N^2-F^2+E^2-m^2$ is just the effective central potential whereas $\frac{1}{F+N}\frac{1}{r}\frac{\partial}{\partial r}(F+N)$, the corresponding spin-orbit piece.

To describe antiproton-nucleus scattering, within the same Dirac eikonal model, we merely replace F_p and N_p of Eqs. (6) and (7) by[1]

$$F_{\bar{p}} = E + V_0^*(\vec{b}, z) \quad (8)$$

$$N_{\bar{p}} = m + V_s^*(\vec{b}, z) \quad (9)$$

We now employ the relations

$$J_0(qb) = \frac{1}{2}\left[H_0^{(1)}(qb) + H_0^{(2)}(qb)\right] \quad (10)$$

$$J_1(qb) = \frac{1}{2}\left[H_1^{(1)}(qb) + H_1^{(2)}(qb)\right] \quad (11)$$

where $H_n^{1(2)}(qb)$ are Hankel functions of order n of the first and second type respectively. Asymptotically, these functions behave as[5]

$$H_h^{1(2)}(x) \xrightarrow[x\gg 1]{} \left(\frac{2}{\pi x}\right)^{1/2} \exp\left[+(-)i\left(x - \frac{h\pi}{2} - \frac{\pi}{4}\right)\right] \quad (12)$$

With (10) and (11) we can write for $F_{p,1}$ and $F_{p,2}$, the following

$$F_{1,p} = F_{1,p}^{(+)} + F_{1,p}^{(-)} \quad (13)$$

$$F_{2,p} = F_{2,p}^{(+)} + F_{2,p}^{(-)} \quad (14)$$

where we have identified,

$$F_1^{(\pm)} = \frac{1}{2}(-iK)\int_0^\infty db\, b\, H_0^{(2)}(qb)\left(e^{t_c(b)}\cosh t_{so}(b) - 1\right) \quad (15)$$

$$F_2^{(\pm)} = \frac{1}{2}(-K)\int_0^\infty db\, b\, H_1^{(2)}(qb)\, e^{t_c(b)}\sinh t_{so}(b) \quad (16)$$

We shall refer to $F^{(+)}$ as the near-side and $F^{(-)}$ the far-side contributions, respectively. We are using nomenclature extensively employed in heavy-ion physics[3]. The above decomposition for p+A scattering has been also extensively discussed by Amado's group at Pennsylvania, where particular emphasis was placed on deriving closed expressions for $F^{(+)}$ and $F^{(-)}$[6]. Here we simply evaluate the amplitudes numerically.

Before presenting our results for p+nucleus and $\bar{p}$+nucleus scattering, we list below several important properties of $F^{(+)}$ and $F^{(-)}$.

1) The near-side amplitude $F^{(+)}$ basically carries information above positive-angle scattering (repulsive forces). Absorption, being able to reflect, enters under this category.

2) The far-side amplitude $F^{(-)}$ is sensitive to negative angle scattering (attractive forces). Absorption, also enters here.

3) In the limit when $t_c(b)$ and $t_{s0}(b)$ are purely real (no nuclear-Coulomb phases), we have

$$F^{(+)} = -F^{(-)*} \tag{17}$$

which is an immediate consequence of the relation $H_n^{(1)} = H_n^{(2)*}$.

The first two properties, can be easily understood within a stationary phase evaluation of the integrals' appearing in Eqs. (15) and (16). We have, for the stationary phase $b_s^{\pm}$, (ignoring the contribution of -1 inside the parenthesis in (15) and, disregarding $t_{s0}(b)$)

$$\pm iq = \frac{d}{db} t_c(b)\Big]_{b_s} \tag{18}$$

Remembering that $q = 2k \sin\frac{\theta}{2}$, therefore $\pm iq = 2ik \sin(\pm\frac{\theta}{2})$, and, accordingly, with $\frac{d}{db} t_c(b)\Big]_{b_s}$ interpreted as a deflection function, one associates the + branch in Eq. (18) with positive angle scattering (repulsion) and the - branch with negative angle scattering (attraction).

In light of the above, let us look at the proton-nucleus and antiproton-nucleus scattering. To be specific we consider $p + {}^{40}Ca$ and $\bar{p} + {}^{40}Ca$ at an incident kinetic energy of 500 MeV. The Dirac impulse approximation optical potentials for the proton[7] and antiproton[1] scattering on ^{40}Ca results in the following effective central potentials

$$\mathrm{Re}\, V_c^{p}(r) = 2.0\,\hat{\rho}(r) + 26.2\left[\hat{\rho}(r)\right]^2 \ (\mathrm{MeV}) \tag{19}$$

$$\mathrm{Re}\, V_c^{\bar{p}}(r) = -582.0\,\hat{\rho}(r) + 26.2\left[\hat{\rho}(r)\right]^2 \ (\mathrm{MeV}) \tag{20}$$

$$\mathrm{Im}\, V_c^{p}(r) = -50.6\,\hat{\rho}(r) - 7.6\left[\hat{\rho}(r)\right]^2 \ (\mathrm{MeV}) \tag{21}$$

$$\mathrm{Im}\, V_c^{\bar{p}}(r) = -210.6\,\hat{\rho}(r) + 7.6\left[\hat{\rho}(r)\right]^2 \ (\mathrm{MeV}) \tag{22}$$

where $\hat{\rho}(r)$ denotes the shape of the vector density of the target nucleus which is assumed to be equal to the scalar density. In all our application below we take $\hat{\rho}(r)$ to be the shape of the density extracted from electron scattering.

Owing to the fact that $\mathrm{Re}\, V_c^{p}(r)$ is repulsive, we expect the near-side amplitude $F^{(+)}$ in $p + {}^{40}Ca$ to be larger

than the far-side one. Further, because of strong absorption (see Eq. (21) and our discussion above) we also expect that $F^{(+)}$ and $F^{(-)}$ will not be so different in magnitude. Opposite to this we expect $\bar{p} + {}^{40}Ca$ elastic differential cross-section to be entirely dominated by $F^{(-)}$ in the small angle (small q) region.

In Figures 1 and 2 we present our result for $|F^{(+)}|^2$ and $|F^{(-)}|^2$ for $p + {}^{40}Ca$ and $\bar{p} + {}^{40}Ca$, respectively. $F^{(+)}$ and $F^{(-)}$ for $p + {}^{40}Ca$ are very close in magnitude and have practically equal slopes. Actually what seems to be happening here is the complete dominance of $\mathrm{Im}\, V_C^p(r)$, especially its $\tilde{\rho}(r)$ term in determining the characteristic of $F^{(+)}$ and $F^{(-)}$. These amplitudes seem to behave roughly like[6]

$$|F_p^{(+)}| \propto e^{-\pi a (q - q_c)} \tag{23}$$

$$|F_p^{(-)}| \propto e^{-\pi a (q + q_c)} \tag{24}$$

with a being the diffuseness parameter of $\tilde{\rho}(r)$. The constant q_c is related to the Coulomb repulsion which pushes $F_p^{(+)}$ upward relative to $F^{(-)}$ by a constant amount (the Coulomb repulsion at high energies act like a prism[3]). Actually $q_c = 2k \frac{\eta/kR}{[1 + (\eta/kR)^2]^{1/2}} \approx \frac{2\eta}{R}$, where η is the Sommerfeld parameter $k \frac{2e^2}{2E}$.

The situation in $\bar{p} + {}^{40}Ca$ (Fig. 2) is completely different. Owing to the very strong attraction (the Coulomb force here adds more attraction!), the far-side amplitude $F^{(-)}$ is pushed well above $F^{(+)}$ in the forward direction, thus favoring a situation of structureless angular distribution,

exactly similar to what is seen in the data. Of course at intermediate values of q, $F_{\bar{p}}^{(-)}$ and $F_{\bar{p}}^{(+)}$ cross, and thus result again in Fraunhoffer oscillations. The reason is, basically that $F_{\bar{p}}^{(+)}$ and $F_{\bar{p}}^{(-)}$ have different slopes [3]. Unfortunately, there is no simple form to describe, analytically, the behaviour of $F_{\bar{p}}^{(+)}$ and $F_{\bar{p}}^{(-)}$, similar to Eqs. (23) and (24).

We present in Fig. 3 and 4, our near-far calculation for the $\bar{p} + {}^{12}C$ system at $k_{\bar{p}} = 446$ MeV/c and $k_{\bar{p}} = 879$ MeV/c, studied recently by Nakumara et. al[2]. The potentials used were the same as those of Ref. 1. Again we notice the predominance of $F_{\bar{p}}^{(-)}$ over $F_{\bar{p}}^{(+)}$ in the angle range considered.

The two examples considered here clearly demonstrate the usefulness of the near-far decomposition made in conjunction with the Dirac treatment of the scattering. For example at $k_{\bar{p}} = 879$ Mev/c, where the near-side is strong enough to interface appreciably with the far-side, giving rise to the oscillatory structure in $\frac{d\sigma}{d\Omega}$, the resemblence to the predominantly absorptive proton scattering angular distribution may easily lead to ambiguous conclusions concerning the $\bar{p}$ + A interaction. The near-far decomposition would certainly help remove some of these ambiguities.

In conclusion, whereas p + A elastic scattering is dominated by absorption, the $\bar{p}$ + A system is predominantly refractive in the small angles region. Analysis of antiproton-nucleus scattering in the small angle region, should supply a direct test of the real part of the Dirac central optical potential, in particular its $\tilde{\rho}(r)$ piece, namely $-\left[\mathrm{Re}\, V_s + \frac{E}{m} \mathrm{Re}\, V_0\right]$. In contrast, the corresponding study of the p + A system should supply the value of a, the

diffuseness of the density.

It would be of great value to perform an analytic study of $\bar{p}$ + A scattering (of the kind performed by Amado[6] on the predoninantly absorptive p + A scattering), a case where nuclear refraction is strong.

REFERENCES

1) M.S. Hussein, B.V. Carlson and M.P. Isidro Filho, Submitted for publication.

2) K. Nakumara, J. Chiba, T. Fujii, H. Iwasaki, T. Kageyama, S. Kuribayashi, T. Sumiyoshi, T. Takeda, H. Ikeda and Y. Takada, Phys. Rev. Lett. 52, 731 (1984).

3) See, e.g., M.S. Hussein and K.W. McVoy, Progress in Particle and Nuclear Physics (D. Wilkinson, Editor), in press.

4) R.D. Amado, J. Piekarewicz, P.A. Sparrow and J.A. McNeil, Phys. Rev. C28, 1663 (1983).

5) M. Abramowitz and I.A. Steguer, Handbook of Mathematical Functions (Dover, New York) 1970.

6) See, e.g., R.D. Amado, Advances in Nuclear Physics (J.W. Negele and J. Vogt, Editors), in press.

7) J.A. McNeil, J.R. Shepard and S.J. Wallace, Phys. Rev. Lett. 50, 1439 (1983).

FIGURE CAPTIONS

Figure 1 - Near-side, $|F^{(+)}|^2$ and far-side, $|F^{(-)}|^2$ contributions to the elastic scattering of p + ^{40}Ca at 500 MeV incident kinetic energy. The potential used is given in Eqs. (19) and (21). Also shown is $|F|^2$ (dashed line)

Figure 2 - Same as Fig. 1 for $\bar{p}$ + ^{40}Ca at 500 MeV. The potential used is given in Eqs. (20) and (22).

Figure 3 - Near-side, $|F^{(+)}|^2$. Far-side $|F^{(-)}|^2$ and total $|F|^2$, elastic scattering cross sections for $\bar{p}$ + ^{12}C at $k_{\bar{p}}$ = 466 MeV/c. The potentials used were taken from Ref. 1.

Figure 4 - Same as Fig. 3 for $\bar{p}$ + ^{12}C at $k_{\bar{p}}$ = 879 MeV/c

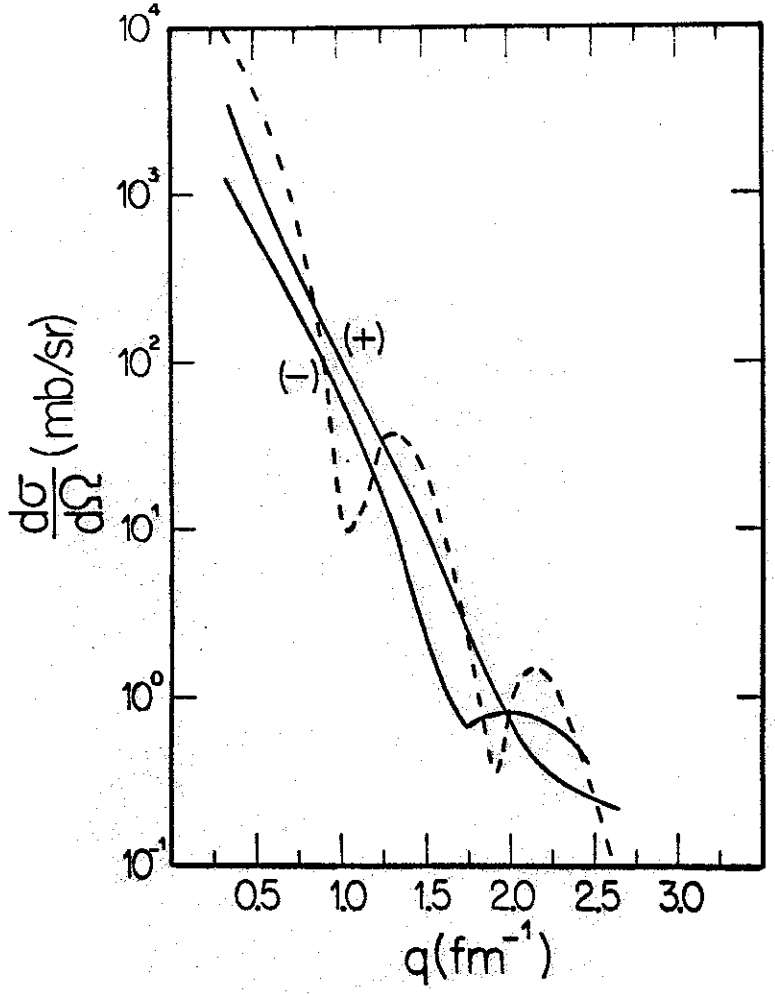

Fig. 1

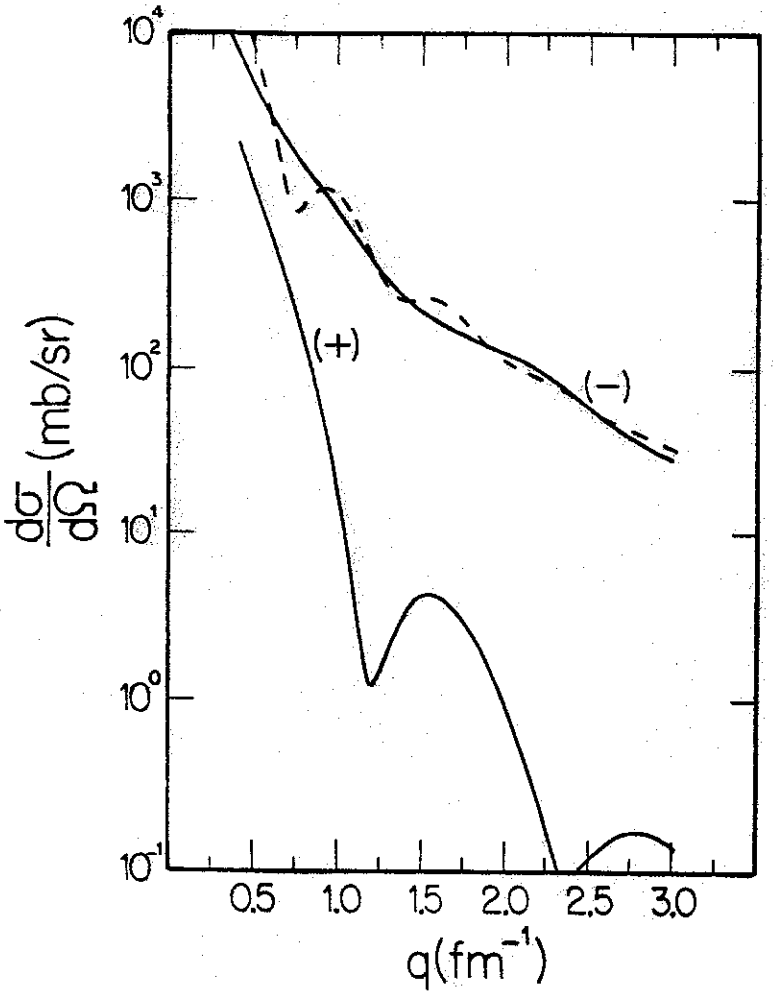
10^4
10^3
10^2
10^1
10^0
10^{-1}
$\frac{d\sigma}{d\Omega}$ (mb/sr)
(+)
(−)
0.5
1.0
1.5
2.0
2.5
3.0
q(fm^{-1})

Fig. 2

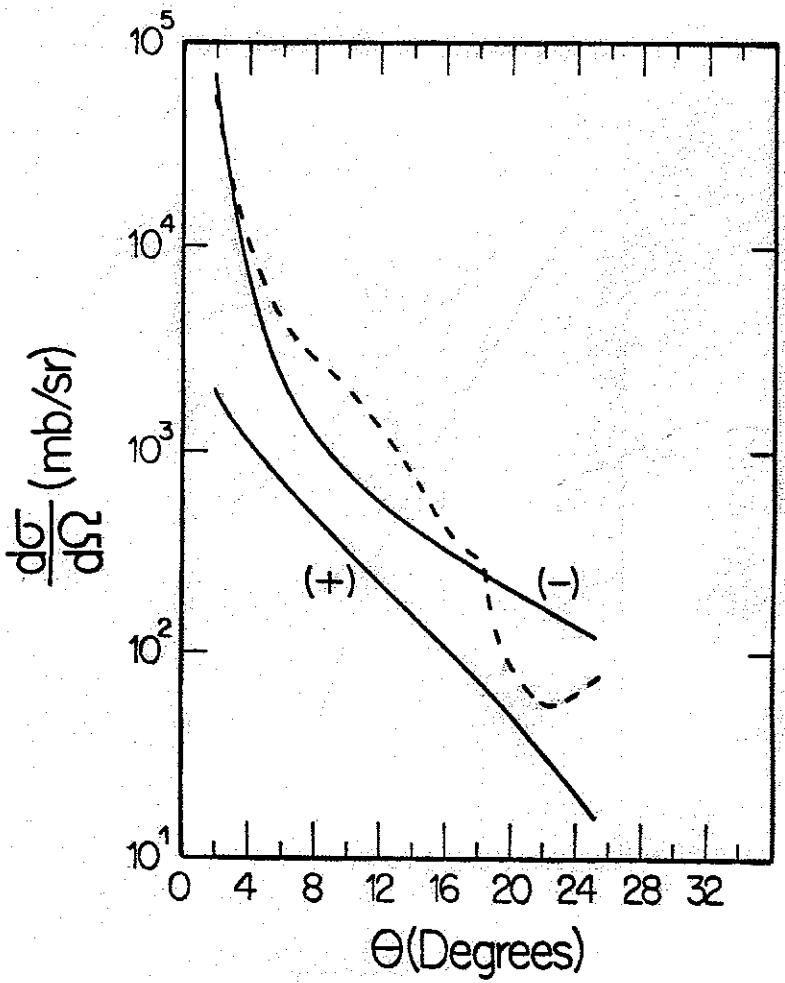
10^5
10^4
10^3
10^2
10^1
$\frac{d\sigma}{d\Omega}$ (mb/sr)
(+)
(−)
0
4
8
12
16
20
24
28
32
Θ(Degrees)

Fig. 3

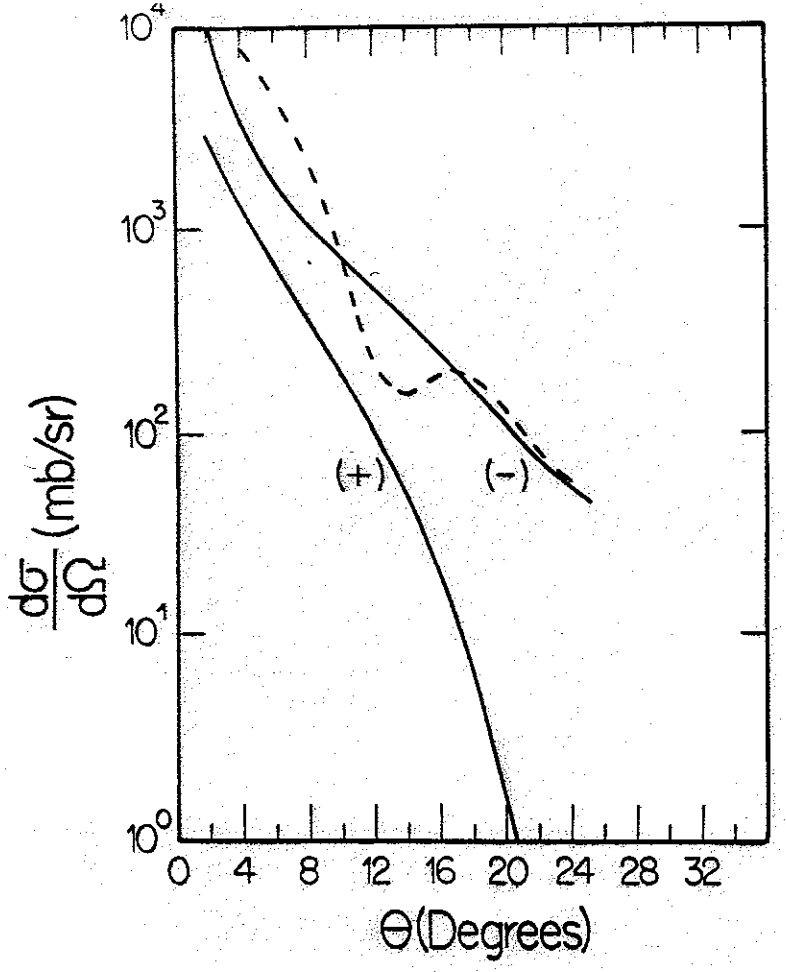
10^4
10^3
10^2
10^1
10^0
$\frac{d\sigma}{d\Omega}$ (mb/sr)
(+)
(-)
0 4 8 12 16 20 24 28 32
Θ(Degrees)

Fig. 4